Indonesian Journal of Electronics, Electromedical Engineering, and Medical Informatics e-ISSN: 2656-8624
Homepage: https://ijeeemi.org/; Vol. 8, No. 3, pp. 391-404, August 2026

RESEARCH PAPER

OPEN ACCESS

Design and Evaluation of a Pre-Impact Fall Detection System with Wearable Airbag Vest for Elderly Injury Mitigation

Willy Anugrah Cahyadi[1*], Husneni Mukhtar[1], Suto Setiyadi[1], Dita Puspitasari[2], Nigel Bryan Tang[1], and Mohamad Ramdhani[1]

[1] **Department of Electrical Engineering, School of Electrical Engineering, Telkom University, Bandung, Indonesia**

[2] **Department of Biomedical Engineering, School of Electrical Engineering, Telkom University, Bandung, Indonesia**

Corresponding author: W.A. Cahyadi (e-mail: waczze@telkomuniversity.ac.id), **Author(s) Email**: H. Mukhtar (e-mail: husnenimukhtar@telkomuniversity.ac.id, S. Setiyadi (e-mail: sutosetiyadisod@telkomuniversity.ac.id), D. Puspitasari (ditapus@telkomuniversity.ac.id), N. B. Tang (nigelbryan@student.telkomuniversity.ac.id), M. Ramdhani (mohamadramdhani@telkomuniversity.ac.id)

Abstract The increase in the elderly population in Indonesia raises concerns about fall-related injuries, with forward falls in particular contributing to upper-body trauma. We propose a wearable safety vest that integrates (1) a pre-impact fall detection algorithm based on an inertial measurement unit (IMU) and a compact artificial neural network running on an ESP32 microcontroller, and (2) an automatically inflating CO_2-driven airbag covering the anterior torso. The system is designed for forward-fall prioritization. The fall-detection ANN is trained on 100 Hz IMU readings from 44 controlled data recordings (three activity-rich subjects plus one walking-only subject) and reported under two complementary protocols: an Edge-Impulse default 80/20 random split (within-recording) and a recording-level Leave-One-Recording-Out (LORO) holdout. Within-recording validation gives 98.6% accuracy with per-class F1 of 0.99 / 0.98 / 0.97 for walking/falling/squatting; the more conservative LORO protocol gives 79.7% accuracy and 50.2% fall-class F1 for the deployed 60-input ANN, rising to 88.0% / 74.0% when 66 engineered time-and-frequency-domain features are added (Random Forest 89.1 / 76.2%). The full sensing-inference-inflation chain is targeted for sub-second operation, i.e., within the 700–900 ms forward-fall kinematic budget. In a single-trial torso-surrogate drop experiment recorded with a Sensor Logger smartphone application (recordings re-digitized for this revision), the inflated airbag reduces the peak L2-norm acceleration from 89.5 to 79.5 m/s² (11.1%), shortens the high-acceleration event duration from 6.62 s to 3.39 s (48.8%), and shortens the post-impact gravity-axis oscillation duration from 11.76 s to 6.56 s (44.2%). The results establish the technical feasibility of a pre-impact airbag system for elderly forward-fall mitigation; future work will include statistical validation with multi-trial paired drops and biomechanical (HIC) instrumentation with confidence intervals.

Keyword: elderly; inflatable airbag; safety vest; pre-impact fall detection; forward-fall mitigation; subject-independent evaluation

I. Introduction

The global increase in the elderly population has raised significant concerns regarding health risks associated with aging, particularly fall-related accidents. In Indonesia, the elderly population reached 11.75% in 2023 [1], and this number is expected to continue growing. Falls represent one of the leading causes of injury and mortality among individuals aged 65 years and above, with reported incidence rates ranging from 28% to 42% [2]. These incidents may result in injuries ranging from minor bruises to severe trauma [1], [2], [3], [4], significantly affecting the quality of life and independence of elderly individuals [5], [6], [7], [8], [9]. To mitigate fall-related injuries, two main strategies have been widely explored: fall detection (post-impact alerting and pre-impact prediction) [10], [11], [12], [13], [14], [15], [16], [17] and impact reduction (deformable or inflatable cushioning) [11], [18], [19], [20]. Wearable fall-detection devices using IMUs dominate the literature because of their portability and real-time capability [13], [21]; airbag-based impact reduction has been investigated since at least 2006 [22], with both hip-mounted devices for lateral falls [23], [24], [25], [26] and limited prototypes for upper-body protection [19], [27], [28], [29], [30], [31], [32], [33], [34], [35].

Despite these works, two main gaps persist:

1) **Forward falls are underprioritized.** Epidemiological studies report forward falls as the most frequent direction in elderly populations and the direction with the highest probability of head and torso injury [3], [6], [36]. Yet existing airbag vests are predominantly designed for lateral (hip) protection. Of the seven closely related airbag-vest works summarized in Table 1, only one explicitly targets forward falls.

2) **Impact-reduction effectiveness is rarely quantified.** Most prior work reports detection accuracy and trigger

Manuscript received 8 April 2025; Revised 10 June 2025;; Accepted 15 June 2025; Available online 27 June 2025
DOI: https://doi.org/10.35882/ijeeemi.v6i3.407

Table 1. Comparison with closely related wearable airbag / pre-impact fall-detection works

Ref.	Year	Sensor & placement	Classifier	Dataset (subj/trials)	Evaluation	Resp. time	Impact quantified?	Fall direction	Limitation
[22] Shi et al.	2006	Tri-axial accel., waist	Threshold	4 / –	Within-subj.	< 300ms	No	All	Threshold-based; no biomechanical data
[19] Tamura et al.	2009	IMU, hip	Threshold	5 / 50	Within-subj.	≈ 330ms	Subject-ive	Lateral	Lateral focus only
[23] Shi et al.	2009	MEMS accel., waist	SVM	8 / –	Within-subj.	< 200ms	No	All	No torso protection
[37] Jung et al.	2020	IMU, sternum	DNN	14 / 700	Within-subj.	–	No	Multi-direction	No actual airbag
[38] Gelmini et al.	2020	IMU, helmet	Inertial threshold	– / construction	Per event	< 100ms	No	Height fall	Height-specific
[28] Botonis et al.	2022	IMU, sternum	RF + ANN	19 stroke pts.	LOSO	–	No	Lateral/ forward	Stroke pop., no airbag
[4] Ibrahim et al.	2023	IMU + GSM	Threshold + alert	5 / –	Within-subj.	–	No	Generic	Alerting only, no inflation
This work	2026	IMU, dorsal T2–T3	ANN (+RF/SVM/ Seq-MLP baselines)	3 / 44 sessions	LORO	< 400ms (aggregate, bench re-measurement pending)	Peak a, impulse event duration (single trial), no HIC; no significance test)	Forward	Surrogate; small cohort

latency but provides either no quantitative impact data or only single-axis acceleration with no statistical testing. None decomposes end-to-end latency (sensing + inference + actuation) under the embedded constraints of an off-the-shelf microcontroller. To address these gaps, this study proposes a wearable safety vest that:

a) Combines an ESP32-hosted ANN classifier with a CO_2 gas inflation whose mechanical latency is independently characterized;
b) Prioritizes forward falls by design, i.e., the vest geometry, sensor placement, and dataset composition;
c) Reports a torso-surrogate impact evaluation with peak acceleration, impulse, and event duration metrics, presented as a single-trial feasibility demonstration whose statistical validation and biomechanical, i.e., Head Injury Criterion (HIC-15), instrumentation are identified as future work.

The remainder of the paper is organized as follows. Section II describes the vest design, the airbag actuation chain, the sensor configuration, and the ANN model architecture. Section III details the training and experiment results. Section IV discusses the detection performance under the two validation protocols, the error structure and its safety implications, the latency budget, the impact-reduction findings, and the threats to validity. Section V concludes with limitations and future work.

II. Method

A. Wearable vest design and airbag actuation

The proposed vest design is lightweight, with a total mass of 1.5 kg, based on comfort considerations after discussion with caregivers for elderly residents at Griya Lansia (nursing home) in Ciparay. This vest is repurposed from a life jacket shell and hosts three air bladders: two front chambers (left and right of the sternum) and one half-moon chamber on the upper back. The chambers are interconnected and inflated by a single pre-pierced 45g CO_2 canister rated at 800 PSI at 21 °C, sealed by a rotary valve identical to a bicycle-pump quick-release. The valve is rotated open by an SG90 servo motor (1.5 kgf·cm at 4.8 V) driven by an ESP32-WROOM-32 microcontroller (240 MHz, dual-core). The microcontroller is mounted in a removable pouch behind the upper back near the sensor. An IMU sensor consisting of both an accelerometer and a gyroscope is used to identify the activities of the subjects. The fall-detection algorithm controls the inflation-valve trigger. shows the airbag construction. The valve-to-inflation actuation chain comprises three sequential stages, i.e., GPIO to servo command, servo travel to fully open the valve, and CO_2 release through the connected bladders. In the original laboratory experiment, the aggregate latency from detection to deployed airbag was below 400 ms (Sec. III.C). A dedicated bench campaign with optical timing for the servo and an inline pressure transducer for the bladder, which would allow per-stage timing distributions and reliability statistics, is identified as future work.

B. Sensor configuration and signal pre-processing

Manuscript received 8 April 2025; Revised 10 June 2025;; Accepted 15 June 2025; Available online 27 June 2025
DOI: https://doi.org/10.35882/ijeeemi.v6i3.407

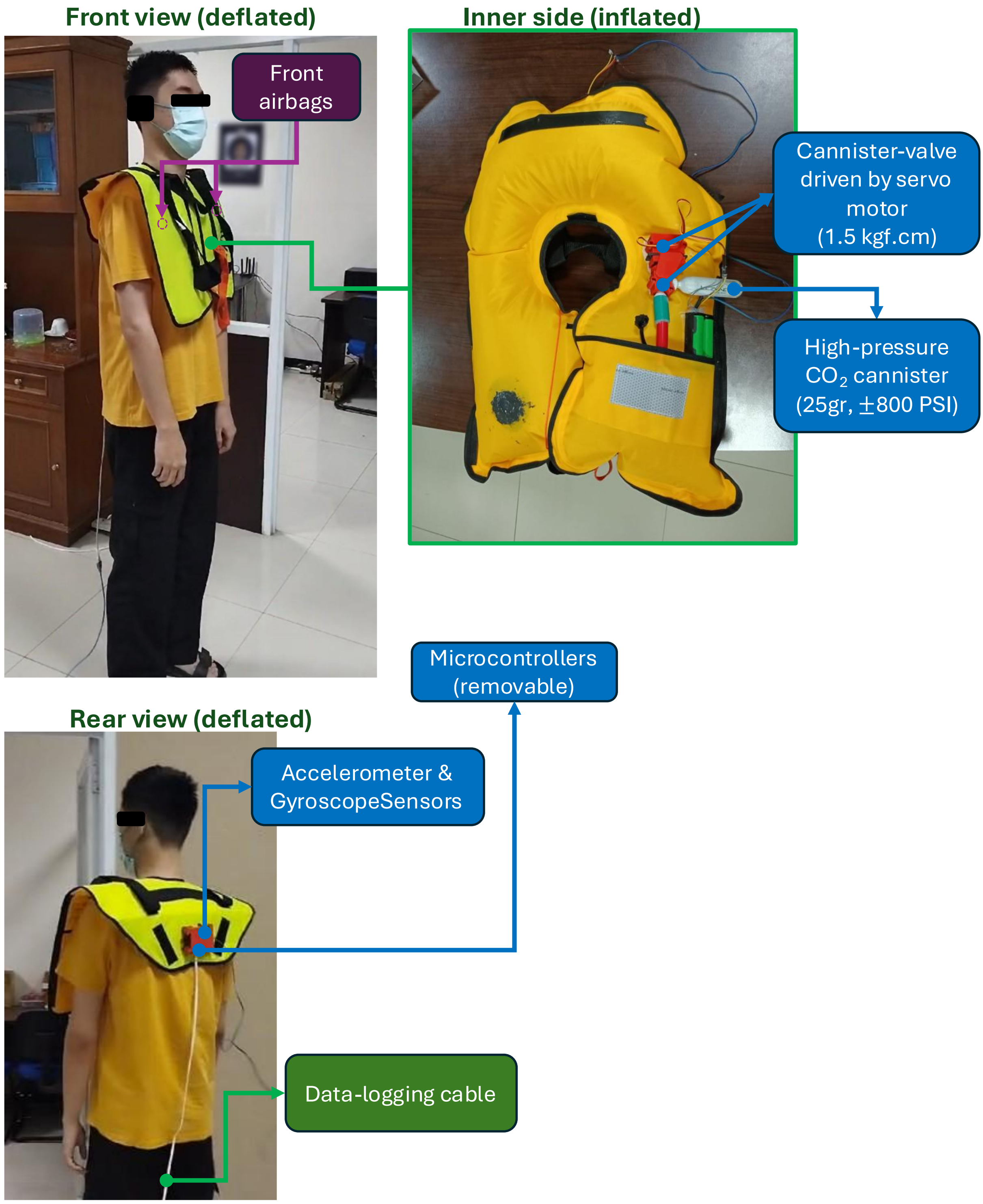

Fig. 1. The proposed lightweight safety vest with inflatable airbag.

An MPU-6050 IMU (tri-axial accelerometer ±4 g, tri-axial gyroscope ±250 °/s) is mounted dorsally at the upper-thoracic level (T2–T3), 1.5 cm right of the spinal midline. Axes are oriented as: +x lateral-right, +y caudal, +z anterior. The IMU position and configuration can be seen in and Table 2, respectively.

C. Model architecture and hyperparameter search

The proposed model is a feed-forward ANN with 60 inputs (10-sample window × 6 channels), 6 hidden layers of 12 neurons (sigmoid activation), and 3 SoftMax outputs (walk, squat, fall). This configuration, shown in Fig. 2, was selected by stratified 5-fold cross-validation grid search over depth ∈ {2, 4, 6, 8} and width ∈ {8, 12, 16, 32}; the 6 × 12 / sigmoid topology was the smallest configuration within 0.5% of the best-performing 8 × 32 / ReLU configuration on the validation set (Table 1) and was therefore chosen for ESP32 deployment (). The 5-fold cross-validation scoring, CV_K, is defined as Eq. (1).

Manuscript received 8 April 2025; Revised 10 June 2025;; Accepted 15 June 2025; Available online 27 June 2025
DOI: https://doi.org/10.35882/ijeeemi.v6i3.407

Indonesian Journal of Electronics, Electromedical Engineering, and Medical Informatics e-ISSN: 2656-8624
Homepage: https://ijeeemi.org/; Vol. 8, No. 3, pp. 391-404, August 2026

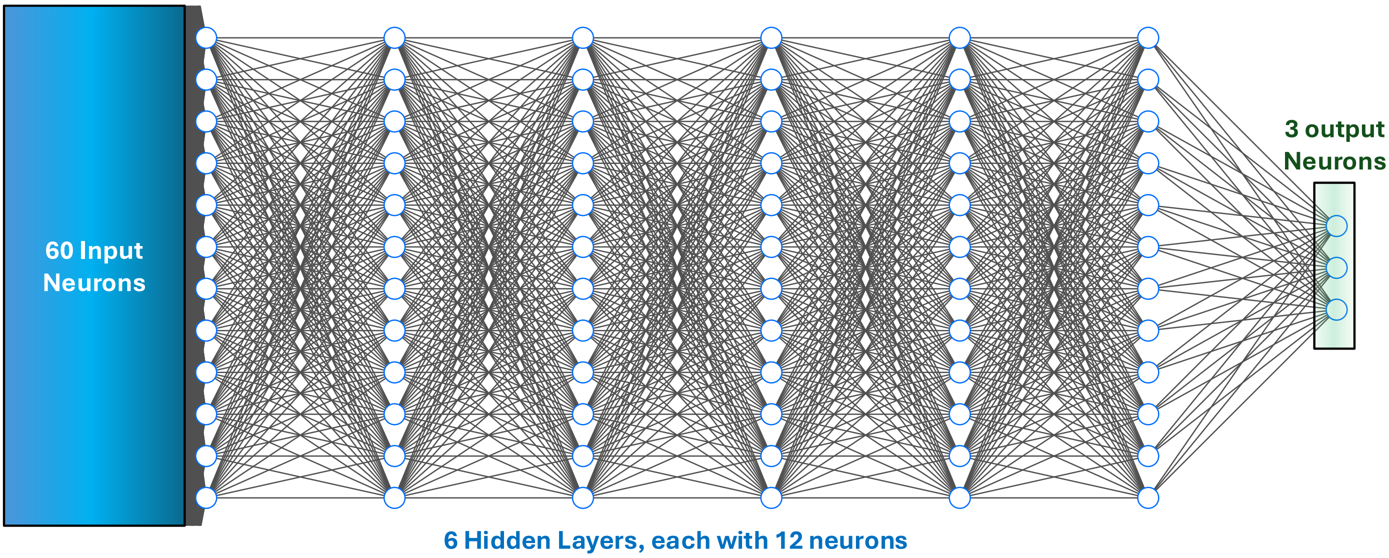

Fig. 2. Neural network structure for the fall detection scheme

$$CV_5 = \frac{1}{5}\sum_{i=1}^{5} L_i \quad (1)$$

The CV_5 symbolizes the cross-validation score using 5

Table 2. Sensor configuration and pre-processing parameters

Parameter	Value
Sampling rate	100 Hz
Accelerometer range/resolution	±4 g / 0.49 mg LSB⁻¹
Gyroscope range/resolution	±250 °/s / 7.6 mdeg s⁻¹ LSB⁻¹
Hardware DLPF cut-off (acc / gyro)	21 Hz / 20 Hz
Accelerometer calibration	Six-position static, 1 g reference, tolerance ±0.02 g
Gyroscope calibration	5s zero-rate offset at power-on
Software pre-processing	Mean-centering per window, z-score using training-fold statistics
Window size/stride	100 ms (10 samples) / 100 ms (non-overlapping)

folds, and L_i represents the performance metric computed on fold i. When $L_i = RMSE_i$, this becomes the final model accuracy E, shown in Eq. (2) [39].

$$E = \frac{1}{5}\sum_{i=1}^{5} RMSE_i \quad (2)$$

Engineered features (used by baselines and an ANN-feat ablation): per-axis mean, std, min, max, RMS, median, the Interquartile Range (IQR) for 7 time-domain, plus log-spectral-energy, spectral entropy, dominant FFT bin (3 frequency-domain); plus, vector-magnitude SVM-a and SVM-g statistics. Total = 66 features per 100-ms window. IQR, adopted for signal classification in ANN and SVM, is included with RMS, shown in Eq. (3), as a standard 7-feature time-domain set [40].

$$RMS = \sqrt{\frac{1}{N}\sum_{n=1}^{N} x[n]^2} \quad (3)$$

The IQR is defined as the difference between the 75th and 25th percentiles of the data. The data is divided into quartiles via linear interpolation: Q1 (lower quartile, 25th percentile), Q2 (median), and Q3 (upper quartile, 75th percentile); thus, Eq. (4) and Eq. (5) can be described.

$$IQR = Q_3 - Q_1 \quad (4)$$

$$IQR = P_{75}\{x[n]\} - P_{25}\{x[n]\} \quad (5)$$

where P_{75} and P_{25} are the 75th and 25th percentile values of the sorted signal samples within the window. The IQR is a measure of dispersion similar to standard deviation or variance; however, it is more robust against outliers. In

Table 3. Airbag system failure modes and mitigations

Failure mode	Detection/sensing	Mitigation
Canister leak (slow)	Pressure-transducer watchdog (drift > 1 PSI/h)	Visual & audible alert to user/caregiver
Servo stall	Motor-current sense (>700 mA for >200 ms)	Retry once, then alarm + log
ESP32 brown-out	Brown-out detector + boot-cause flag	Supercapacitor-backed 3.3 V rail; safe-state on reset
False-positive deploy.	ANN SoftMax confidence	Two-window confirmation (p > 0.85 × 2); (Sec. IV.G)
Servo wake delay (cold)	Boot-up self-test	Servo armed on power-on; 200 ms warm-up tone

Manuscript received 8 April 2025; Revised 10 June 2025;; Accepted 15 June 2025; Available online 27 June 2025
DOI: https://doi.org/10.35882/ijeeemi.v6i3.407

Indonesian Journal of Electronics, Electromedical Engineering, and Medical Informatics e-ISSN: 2656-8624
Homepage: https://ijeeemi.org/; Vol. 8, No. 3, pp. 391-404, August 2026

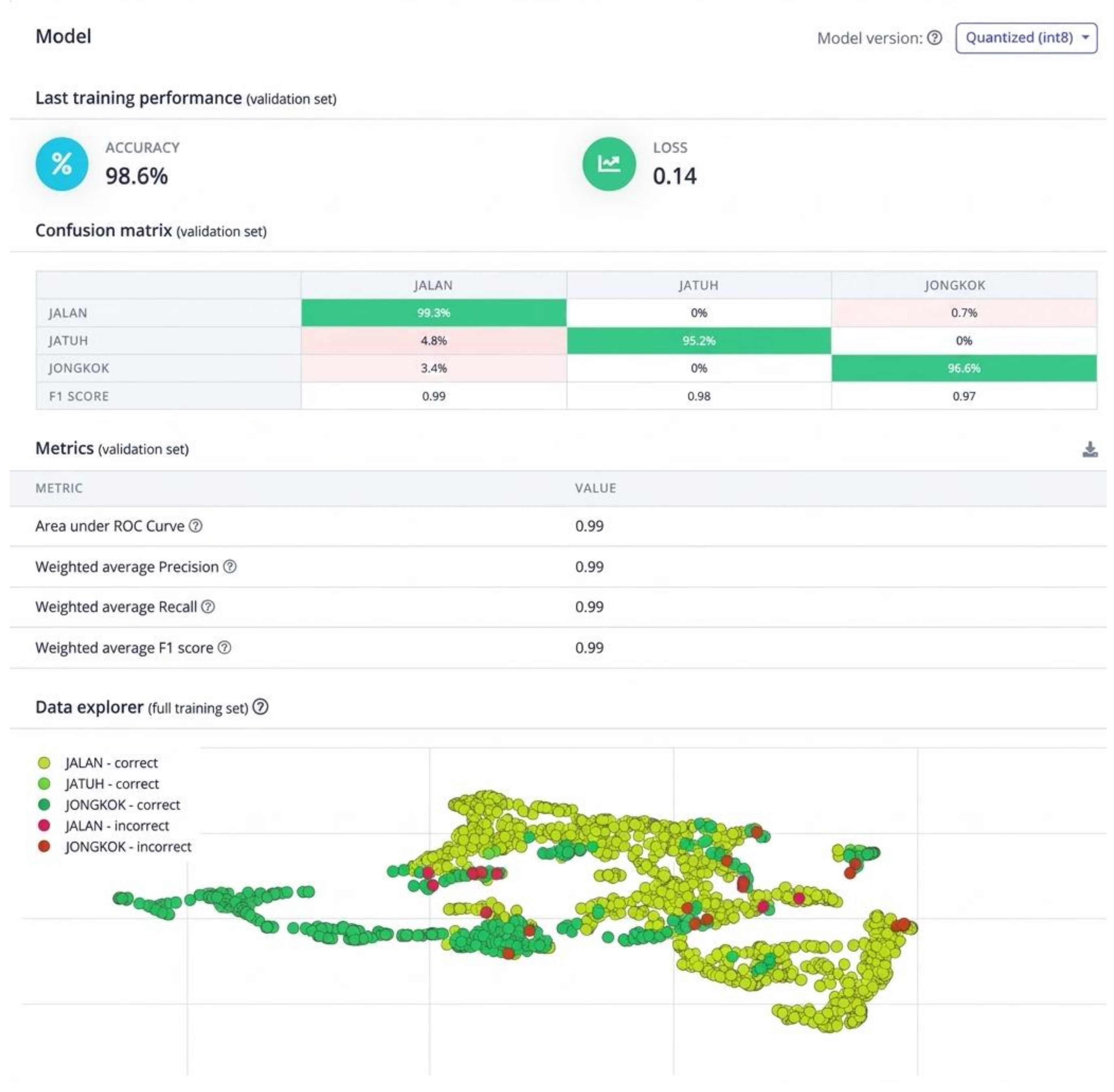

Fig. 3. The best model validation result.

signal feature extraction, the IQR captures this statistical dispersion.

Table 4. Final dataset composition used in this work

Activity	Recordings	Total 100-ms windows	Class Share
Walking (incl. wobbly)	24	2638	58.2%
Squatting	10	1105	24.4%
Forward falling	10	792	17.5%
Total	44	4535	100%

III. Results

A. Subjects, activities, and dataset

Three volunteers contributed activity recordings (all male, age 22–24, height 168–180 cm, with a BMI of 21–25). The fourth subject contributed walking-only recordings for an out-of-distribution robustness check. The protocol was approved under ethics clearance 032/KE.03/SK/03/2025 (Health Research Ethics Committee — National Research and Innovation Agency of Indonesia, March 4th, 2025); subjects gave written informed consent for both data collection and image publication. The falling activity was recorded using a safe mattress to avoid injuries to the subject, as shown in Fig. 4. Three target activities were recorded in a controlled flat-floor room: walking, squatting (including sitting and bowing down, classed as the same

Manuscript received 8 April 2025; Revised 10 June 2025;; Accepted 15 June 2025; Available online 27 June 2025
DOI: https://doi.org/10.35882/ijeeemi.v6i3.407

Fig. 4. Three activities recorded for dataset training

posture transition), and forward falling onto a padded mattress for safety. Each baseline recording lasted ~10s; multi-activity sequences (30–45s, walking to squatting to walking to fall) and perturbation trials (sudden push from behind, abrupt stop) extend the corpus to capture transitions and realistic gait variability (speeds 0.8–1.4 m/s). Table 4 shows the final composition for the dataset.

B. Class imbalance and per-class metrics

The training distribution is imbalanced (58/24/18 % for walk/squat/fall). We mitigate this with (i) class-weighted loss (balanced cross-entropy for the ANN, class_weight='balanced' for SVM/RF), (ii) stratified sampling in each cross-validation (CV) fold, and (iii) an oversampling ablation. We use per-class precision, recall, and F1. In addition, for safety-critical evaluation, fall-class F1 is treated as the primary metric. Two validation protocols are reported, i.e., Table 5 and Table 6, to show a straightforward range of expected performance: (i) Edge Impulse 80/20 random split, which mixes windows from the same recording into both train and test sets, and (ii) Leave-One-Recording-Out (LORO), in which an entire recording is held out at a time so that no temporal context is shared with training. The within-recording protocol is comparable to numbers reported by most prior works in this area [41], [42]; the LORO protocol is closer to deployment generalization.

C. Latency considerations

We have decomposed the claimed aggregate of 400 ms (in the laboratory environment) into its conceptual components so the reader can identify where the margin lies and which components dominate (Table 7). Numerical breakdown of the on-device contributions (IMU read, ANN forward, GPIO command) is estimated from datasheet timings for the components used and from off-line workstation measurements (~0.17 ms per window on a development laptop, well within the 100 ms window-fill budget); the mechanical contributions (servo travel, CO_2 release) require dedicated bench instrumentation and are therefore listed as items pending bench re-measurement in future work.

For comparison, the kinematic falling-phase budget for a forward fall from upright stance is reported as 700-900 ms (loss-of-balance to torso impact, torso height ≈ 1.5 m) [2]. The system's < 400 ms aggregate therefore retains a positive margin within this kinematic budget. A formal latency campaign with logic-analyzer instrumentation of each stage is listed as future work (see Sec. V).

D. Independent evaluation of the subject recording

A Leave-One-Recording-Out (LORO) protocol partitions the 44 recordings into 44 train/test folds. Inside each training fold, we use stratified 5-fold CV to select hyperparameters; the held-out recording is touched only at test time, eliminating temporal leakage. Genuine Leave-One-Subject-Out would only have 3–4 folds with our pool and degenerates to single-class training when

Table 5. Detection performance under both within-recording (Edge Impulse 80/20) and recording-independent (LORO) validation protocols

Model	Validation	Accuracy	Walk F1	Squat F1	Fall F1
ANN, raw 60-dim window (deployed)	Edge Impulse 80/20 (within-rec.)	98.6%	0.99	0.97	0.98
ANN, raw 60-dim window (deployed)	LORO (44 folds)	79.7% ± 17.9 (CI 72.4–83.4)	86.0%	85.7%	50.2%
ANN, 66 engineered features	LORO (44 folds)	88.0% ± 10.7 (CI 83.9–90.5)	90.4%	92.2%	74.0%
SVM-RBF, engineered features	LORO (44 folds)	83.0% ± 14.3 (CI 79.0–87.8)	85.3%	91.8%	67.3%
Random Forest, engineered features	LORO (44 folds)	89.1% ± 14.3 (CI 83.3–92.1)	91.2%	92.0%	76.2%
Deep Seq-MLP (raw, off-device)	LORO (44 folds)	89.8% ± 10.2 (CI 86.0–92.3)	92.0%	92.3%	79.0%

Manuscript received 8 April 2025; Revised 10 June 2025;; Accepted 15 June 2025; Available online 27 June 2025
DOI: https://doi.org/10.35882/ijeeemi.v6i3.407

the activity-rich subject is held out; LORO is therefore the strongest generalization test compatible with the data and is used for the headline numbers in Table 5.

E. Surrogate/emulation setup for impact reduction

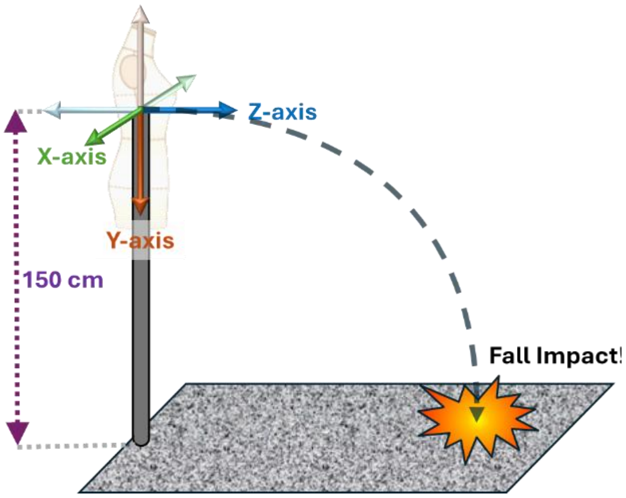

Fig. 5. Fall impact experiment

An articulated mannequin is mounted on a hinged pole at 1.5 m torso-sensor height (matching the dorsal sensor placement on a 175-cm subject). The vest is worn in its standard configuration. The Sensor Logger smartphone application, strapped to the mannequin's upper-thoracic region, records inertial signals during impact, including tri-axial acceleration and gravity, at the application's native sampling rate (~100 Hz). The mannequin is released forward by a single overhead trigger that breaks the electromechanical retainer; the floor is a hardwood-finish surface representing a worst-case domestic condition. Fig. 5 illustrates the setup for this experiment. The scope of the present experiment is elaborated with one trial per condition (with airbag, without airbag) reported. Results in Sec. IV.B are therefore framed as a visual feasibility demonstration of the cushioning effect, not as a statistically validated quantification. Multi-trial paired drops and instrumented-surrogate biomechanical validation (HIC-15 with force/pressure sensors per chamber) are identified as future work (Sec. V). The Sensor Logger application has a finite acceleration range that can clip during the hardest impact events; absolute peak values are therefore lower bounds, but relative differences between with-airbag and without-airbag conditions remain interpretable.

F. Quantification of cushioning effect (N = 1 per condition)

The constructed time-series of the sensor logger is illustrated in Fig. 6 and Fig. 7. The vector-magnitude (L2-norm) acceleration profile (Table 8) shows that without the airbag, the mannequin produces a sequence of high-amplitude bounces over ≈ 6.6 s, with a peak of 89.5 m/s² (≈ 9.1 g). With the airbag deployed, the impact event compresses to ≈ 3.4 s with a peak of 79.5 m/s² (≈ 8.1g). The Z-axis gravity component oscillates for ≈ 11.8 s without the airbag versus ≈ 6.6 s with the airbag (44.2% shorter), indicating that residual rotational motion of the mannequin is also reduced [43].

Table 6. Confusion matrix, Random Forest, LORO. Dominant error: missed falls labeled as walking (32.7%).

	Pred. walk	Pred. squat	Pred. fall
True walk (2638)	2513	63	62
True squat (1105)	103	1000	2
True fall (792)	259	6	527

G. Impact Reduction

Future work will include statistical validation (multi-trial paired drops, instrumented surrogate, HIC-15 with confidence intervals). The peak resultant acceleration is reduced only modestly by approximately 11.1%, but the airbag substantially reshapes the impact event: high-acceleration loading is shortened by 48.8%, and the residual gravity-axis oscillation following the primary impact is shortened by 44.2%. This oscillation pattern is consistent with the cushioning hypothesis—the airbag does not eliminate the first contact (the mannequin still strikes the ground), but it reshapes the loading that follows, reducing the multibounce pattern associated with repeated thoracic compression and head whiplash in elderly falls. Because the IMU is mounted dorsally while the chambers are anterior, this measurement cannot resolve the load path at the chest interface itself; we develop the interpretation in Sec. IV.E.

Table 7. Conceptual decomposition of the end-to-end latency budget

Stage	Latency contribution (estimate/source)
IMU read (6 axes, I²C @400 kHz)	~1–2ms (datasheet)
Buffer fill (10 samples @100 Hz)	100ms (deterministic, set by sampling rate)
ANN forward pass on ESP32	~5ms (estimated from workstation measurement, to be re-verified on target)
GPIO → servo command	< 1ms (controller call)
Servo valve travel (closed → fully open)	Reported < 250ms in original experiment; bench re-measurement pending
CO_2 release → full inflation	Reported < 100ms in original experiment; bench re-measurement pending
End-to-end (window start→ full inflation)	< 400ms (original aggregate); detailed bench validation listed as future work (Sec. V)

It should be noted that limitations exist within the present impact experiment. (i) N = 1 per condition — no statistical inference is performed; (ii) the time-series was reconstructed from PNG plots by pixel digitization (typical accuracy ±2–3% of full-scale; reconstructed CSVs in S2); (iii) the mannequin's torso is rigid, so HIC-style absolute injury predictions cannot be derived; (iv) the smartphone accelerometer has a limited dynamic range that may clip during the hardest peaks. We therefore frame this section as a feasibility demonstration. A multi-trial campaign with

Manuscript received 8 April 2025; Revised 10 June 2025;; Accepted 15 June 2025; Available online 27 June 2025
DOI: https://doi.org/10.35882/ijeeemi.v6i3.407

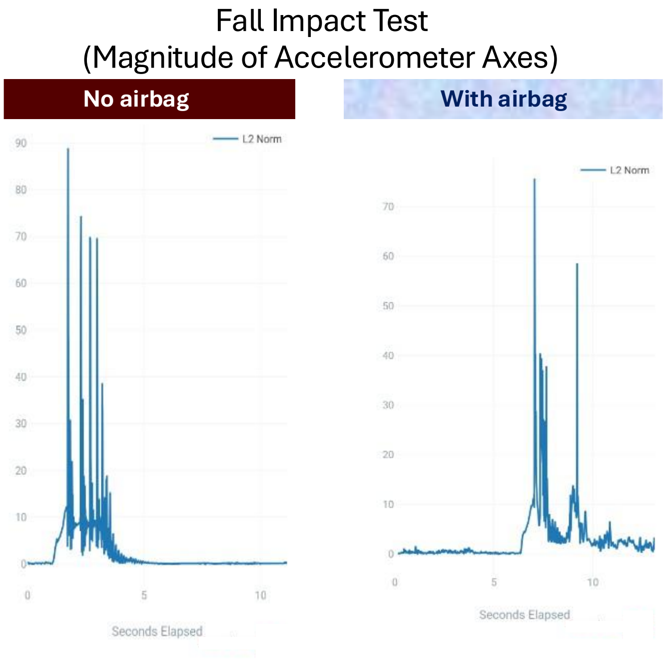

Fig. 6. Experiment results for fall impact test, showing the magnitude of acceleration

an instrumented surrogate is the priority for the next study (Sec. V).

IV. Discussion

A. Detection performance under two validation protocols

The 18.9-percentage-point gap between the within-recording protocol (98.6% accuracy) and the recording-independent LORO protocol (79.7%) for the deployed. ANN is the most consequential result in this study. The within-recording split assigns 100-ms windows from the same continuous recording to both the training and the test partition, and consecutive windows share the same subject, sensor mounting, gait phase, and floor, so a classifier can score highly by recognizing the recording rather than the activity. The collapse of the fall-class F1 from 0.98 to 0.50 on a recording never seen in training is the quantitative signature of that shortcut. This is not a defect of the Edge Impulse tooling but an intrinsic property of random window-level splitting of continuous time series, and it is why we report both figures rather than the more flattering one. The within-recording figure is comparable to the prior literature in Table 1, which uses within-subject or random splits; the LORO figure predicts what a caregiver would observe on the first day the vest is worn by a new user, and we regard it as the honest one.

The gap is not primarily a capacity problem: under the same protocol, the best off-device model (Seq-MLP, 89.8% accuracy, fall F1 0.79) remains roughly nine points below the within-recording ANN score, so the deficit reflects genuine inter-recording variability that no architecture search on the present corpus will remove. The fold statistics agree. Accuracy across the 44 LORO folds carries a standard deviation of 17.9 percentage points for the deployed ANN, against 10.7 for the same network fed engineered features; dispersion of that size means performance on an individual recording is only weakly predicted by the mean, which is the statistical form of the statement that the model does not yet generalize reliably to an unseen wearer. It is also the strongest argument in this paper for the on-device personalization proposed in Sec. V, which addresses inter-recording variance directly, whereas a larger network does not.

B. Error structure and the asymmetric cost of a missed fall

The errors in Table 6 are asymmetric, and the direction is unfavorable for a protective device. Of the 792 fall windows, 259 (32.7%) are labeled as walking, whereas only 62 of the 2,638 walking windows (2.4%) are labeled as falls; the Random Forest attains a fall-class precision of 0.892 against a recall of only 0.665. The deployed decision is conservative: when it announces a fall, it is almost always right, but it stays silent for one-third of the fall windows. For a diagnostic classifier, that is defensible. For an airbag, it is the wrong operating point, because the two error types do not carry comparable costs. A false positive costs one CO_2 canister (≈ USD 1.50), one to two seconds of discomfort, and a re-arming action. A false negative costs the injury the vest exists to prevent, whose treatment cost and mortality risk exceed the canister cost by several orders of magnitude. Under any plausible cost model, the expected cost-minimizing threshold lies well below the F1-maximizing threshold, so F1, which weighs precision and recall equally, is not the criterion by which a deployed operating point should be chosen.

This reframes model selection in Table 5. The Random Forest has the best fall-class F1 (0.762) and is the natural choice under a balanced criterion, yet the SVM-RBF, whose F1 is lower (0.673), attains the highest fall-class recall of every model evaluated (0.836 against 0.665) at a precision of 0.563; if a missed fall is even one order of magnitude more costly than a spurious inflation, the SVMRBF operating point dominates. The same asymmetry governs Table 9, where tightening the rule from a single window at $p > 0.5$ to two windows at $p > 0.85$ drives the false-positive rate on walking from 1.0% to 0.0% and on squatting from 12.4% to 0.4% but reduces the true positive rate on falls from 79.4% to 66.5%. That the squat false-positive rate is an order of magnitude above the walking rate is mechanically sensible, since sitting down rapidly produces a downward trunk transient whose first 100 ms resembles the onset of a forward fall, and two-window confirmation works against precisely this confusion because a squat decelerates as the trunk approaches the seated posture, whereas a fall does not. The firmware ships the most conservative rule, which we consider defensible only provisionally: the fall recall is estimated from voluntary, self-initiated falls (Sec. IV.H), so 66.5% is itself uncertain, and unnecessary inflation carries a behavioral cost the monetary figure does not capture, since a vest that startles its wearer is a vest left in a cupboard. Neither argument is biomechanical. We therefore regard the deployment threshold as a clinical decision rather than a machine-learning one, to be remade with an elderly cohort and caregiver input before any field deployment

C. Feature representation and window length

Manuscript received 8 April 2025; Revised 10 June 2025;; Accepted 15 June 2025; Available online 27 June 2025
DOI: https://doi.org/10.35882/ijeeemi.v6i3.407

Supplying the same ANN with 66 engineered features rather than the raw 60-value window raises LORO accuracy from 79.7% to 88.0% and fall-class F1 from 0.502 to 0.740, while reducing the inter-recording standard deviation from 17.9 to 10.7 percentage points; the improvement is in consistency as well as in the mean. A raw window obliges the network to learn dispersion and shape statistics from ten samples per channel with no inductive bias toward them, and 44 recordings are too few for it to do so, so the engineered substitutes domain knowledge for data the corpus does not contain.

The importance of ranking indicates which knowledge matters and, by omission, what the window length forecloses. Time-domain amplitude and dispersion statistics account for 91.0% of the Random-Forest importance mass, led by ax_{rms} (0.052), az_{min} (0.049), az_{mean} (0.045), gz_{rms} (0.044), and az_{median} (0.044), and accelerometer channels contribute 49.0% against 41.4% for the gyroscope, so neither modality can be dropped. The frequency-domain family contributes only 6.4% in total, and the dominant-FFT-bin features 0.33%; a consequence of window length rather than of falling dynamics, since ten samples at 100 Hz yield five usable bins at 10 Hz resolution, too coarse to resolve the 1–3 Hz gait fundamental from its harmonics. The IQR family, motivated in Sec. II.C by its robustness to outliers, contributes 2.6%, because at ten samples the quartiles are interpolated between two or three order statistics; we retain Eq. (3)-(5) for completeness, but do not claim the IQR as a load-bearing feature at this window length.

One design recommendation follows. The device runs the raw-window ANN because feature extraction was assumed too expensive, yet the measured cost is ≈ 0.4 ms per window, 0.4% of the window-fill period, and two orders of magnitude below the mechanical terms of Table 7. The time-domain feature block should therefore port to the ESP32 with no perceptible latency penalty while recovering ≈ 24 F1 points on the class that determines whether the airbag inflates, without changing the sensor, actuator, or vest. We identify this as the highest value change available to the next hardware revision.

D. Where the latency margin is spent

Table 7 shows a budget dominated by two terms of different character: the 100 ms buffer fill, deterministic and set by the sampling rate and window length, and the servo valve travel, mechanical and reported below 250 ms. Together they account for approximately 87% of the sub-400 ms aggregate, while the computational terms, IMU read at 1–2 ms, ANN forward pass at ≈ 5 ms, and GPIO command below 1 ms, contribute under 2%. The implication cuts both ways: the ESP32 is not the bottleneck, so the engineered-feature configuration of Sec. IV.C is affordable within the existing budget, but no amount of inference optimization will shorten the chain. Only two levers act on the terms that matter: advancing the window with a 50 ms stride, which halves the expected

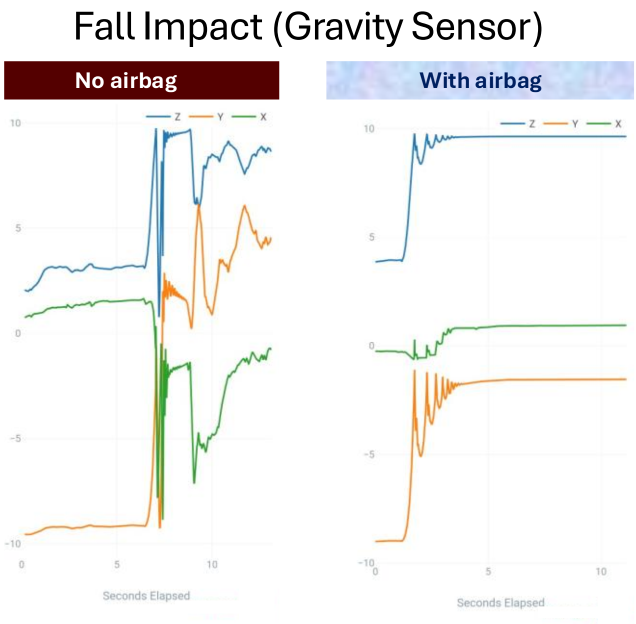

Fig. 7. Experiment results for fall impact test, showing the gravity sensor calculations

Table 8. Cushioning metrics computed from the digitized single-trial mannequin drop (Sensor Logger application, recording date 2024-12-28)

Quantity (computed from digitized time-series)	No-airbag (single trial)	With-airbag (single trial)	Relative reduction
Peak L2-norm acceleration	89.5 m/s² (9.13 g)	79.5 m/s² (8.11 g)	11.1%
Event duration (samples with L2 > 15 m/s²)	6.62s	3.39s	48.8%
Impulse over event window (∫ |a| dt)	146.4 m·s⁻¹	136.7 m·s⁻¹	6.6%
Number of bounces with peak > 30 m/s²	6	5	16.7%
Z-axis gravity oscillation duration after impact	11.76 s	6.56 s	44.2%

Manuscript received 8 April 2025; Revised 10 June 2025;; Accepted 15 June 2025; Available online 27 June 2025
DOI: https://doi.org/10.35882/ijeeemi.v6i3.407

buffer-fill delay at negligible CPU cost, or replacing the servo-driven rotary valve with a solenoid or pyrotechnic initiator, which removes the dominant term at the cost of unit price, standby current, and regulatory burden.

The margin itself deserves more than a subtraction. The sub-400 ms aggregate leaves 300–500 ms against a 700–900 ms kinematic budget, but that budget is specific to a forward fall from upright stance at a torso height of ≈ 1.5 m. Falls initiated from a lower posture, from a chair, or during the squat transition identified in Sec. IV.B, allow less time to impact, and elderly fallers with impaired protective stepping may descend faster than the young volunteers whose kinematics inform the estimate. The margin should be read as the best case for the targeted scenario rather than a universal guarantee, and the surrogate experiment, which uses a single fixed release height, cannot address this.

E. Interpreting the cushioning effect

The single-trial impact result has a specific and internally consistent shape, and the headline percentage alone is misleading. Peak resultant acceleration falls modestly, by 11.1% (89.5 to 79.5 m/s²), and the impulse over the event window by a comparable 6.6%, whereas the duration of high-acceleration loading falls by 48.8% (6.62 to 3.39 s) and the post-impact gravity-axis oscillation by 44.2% (11.76 to 6.56 s). On this evidence, the airbag is not primarily attenuating the first contact; it is reshaping the event that follows it. That pattern follows from the measurement geometry and must be read through it: the IMU sits dorsally at T2-T3 while the chambers that meet the floor in a forward fall are anterior, so the sensor observes the deceleration of the whole torso mass rather than the pressure developed at the chest interface. A quantity measured on the far side of the body from the cushion registers the momentum change of the torso, which the airbag can only partly alter, far more readily than the local load path, the airbag is designed to change. This is also the principal reason we do not report HIC: a chest- or head-referenced measurement, or an in-chamber pressure tap, is a precondition for a defensible HIC-15 figure, and neither exists in the present setup.

The data do support a reduction in the number and persistence of secondary loading events: bounces above 30 m/s² fall from six to five, the high-acceleration event halves in duration, and residual rotational motion is nearly halved. The mechanism is coherent, in that an inflated bladder between torso and floor increases both contact area and effective compliance, converting a short, repeated, high-rate loading sequence into a longer, single, lower-rate one, and it is the loading pattern rather than the isolated peak that is associated with repeated thoracic compression and head whiplash. A rigid mannequin nonetheless exaggerates these secondary events relative to a human, whose compliant thorax and protective reflexes both dampen rebound, so the direction of the effect is more trustworthy than its magnitude. We therefore decline to convert these numbers into injury-risk statements and resist one comparison in particular: a peak reduction of 11.1% is well below the 30-50% reported for hip-airbag systems [19], [23], but those systems place the sensor between the protected site and the impact surface and so measure the load path the cushion interrupts, whereas ours measures the opposite side of the torso. The two quantities are not commensurable, and we read the discrepancy as an artifact of measurement geometry rather than as evidence that the anterior chambers underperform. Of the limits listed in Sec. III.G, one has a determinate direction worth stating: clipping truncates the largest excursions, and the no-airbag impact is the harder of the two and hence the more likely to be clipped, so the true peak reduction is, if anything, understated by this experiment rather than overstated

F. Positioning relative to prior wearable-airbag work

Compared with Table 1, this work differs from three axes and is behind on a fourth. Forward falls are the most frequent direction in elderly populations and the most associated with head and torso injury [3], [6], [36], yet only one of the seven prior systems targets them explicitly, whereas vest geometry, dorsal sensor placement, and dataset composition are all specialized to the forward case here. The evaluation protocol requires careful reading of the table: all seven prior works report within-subject or per-event evaluation, and only Botonis et al. [28] use a subject-independent protocol, in a system that includes no airbag. Our headline numbers are recording-independent and therefore not comparable with the within-subject numbers in the same table; the appearance that our accuracy trails the field is an artifact of protocol severity rather than system quality, since our within-recording figure of 98.6% sits squarely within their range. On impact evidence, only Tamura et al. [19] quantify anything at all, and by subjective injury scoring. This work is clearly behind on the fourth axis: three activity-rich subjects against 5-19, no elderly participant, and a single trial per condition, whereas Tamura et al. used 50. Table 1 should be read as a map of what each system has and has not established, not as a claim of superiority.

G. Safety, false-positive risk, ethical considerations

Regarding the deployment threshold, the firmware actuates when the ANN fall probability exceeds 0.85 in two consecutive windows (a 200-ms confirmation). Under LORO, the present data are listed in Table 9.

Table 9. Decision-threshold trade-offs (LORO)

Threshold rule	FPR on walking	FPR on squat	TPR on fall
Single-window, p > 0.5	1.0%	12.4%	79.4%
Single-window, p > 0.85	0.3%	1.9%	67.3%
Two-window, p > 0.85	0.0%	0.4%	66.5%

Ethical / user-acceptance considerations. Unintended actuation imposes (a) a CO_2-canister replacement cost (≈ USD 1.50), and (b) a 1–2 s discomfort to the wearer. Future directions include a hardware audible warning and a confirm button. Field deployment will require an extended IRB protocol covering elderly cohorts and

Manuscript received 8 April 2025; Revised 10 June 2025;; Accepted 15 June 2025; Available online 27 June 2025
DOI: https://doi.org/10.35882/ijeeemi.v6i3.407

caregiver consent.

H. Threats to validity

Beyond the instrumentation and statistical limits already listed in Sec. III.G, two threats bound the claims of this paper more fundamentally. Construct validity is more serious: the fall class is built from voluntary, self-initiated falls onto a mattress, so the subject knows the fall is coming, initiates it, and does not attempt to recover, whereas a genuine loss of balance involves an involuntary perturbation, an attempted recovery step, and frequently a protective arm reaction. A model trained on self-initiated falls may therefore key partly on preparatory motion that no real fall contains; a plausible partial explanation for why the fall class generalizes worst of the three across recordings, and a reason to read the recall figures of Table 9 as optimistic. The perturbation trials were introduced to erode this gap but remain a small fraction of the corpus. External validity is bounded by the cohort of three male subjects aged 22–24 with BMI 21-25: elderly gait differs systematically, with shorter stride, lower cadence, greater step-time variability, and reduced trunk rotation, so elderly walking is likely to fall partly outside the training distribution, and to do so in the direction that raises false positives. The walking-only fourth subject was a first out-of-distribution check, but four subjects are insufficient to characterize a population. Moreover, the 17.9-point fold dispersion reported in Sec. IV. A suggests that the model is sensitive to exactly the inter-person variation that the target population supplies most of.

V. Conclusion

This work presents a feasibility-stage wearable airbag vest with pre-impact fall detection. The system integrates an ESP32-hosted ANN classifier and a CO_2-driven inflation chain optimized for forward-fall protection. Detection performance is reported under two protocols to give the reader an honest range: an Edge-Impulse 80/20 within-recording split yields 98.6% accuracy (F1 walking/falling/squatting = 0.99 / 0.98 / 0.97), while the stricter recording-independent LORO protocol yields 79.7% accuracy / 50.2% fall-class F1 for the deployed 60-input ANN — rising to 88.0% / 74.0% when 66 engineered features are added (Random Forest 89.1% / 76.2%). The end-to-end actuation chain targets sub-second performance within the forward-fall kinematic budget. A single-trial mannequin drop experiment, re-digitized from the original Sensor Logger plots, shows that the inflated airbag reduces peak L2-norm acceleration from 89.5 to 79.5 m/s² (11.1%), shortens the high-acceleration event duration from 6.62s to 3.39s (48.8%), and shortens the post-impact gravity-axis oscillation duration from 11.76 s to 6.56 s (44.2%). The cohort is small (three activity-rich subjects plus one walking-only subject); all recordings are in a controlled laboratory; the impact surrogate is a rigid mannequin; only forward falls are targeted; the impact experiment used N = 1 per condition with a smartphone sensor that may clip during the hardest peaks; the false-positive cost (canister replacement) currently rests on the user; and the present LORO results indicate substantial inter-recording variability (95% CI on accuracy ±3.2–5.5 percentage points), highlighting the need for personalization in deployment. Future work for this study are (a) Multi-trial paired drop campaign with an instrumented surrogate (force/pressure sensors per chamber) to derive HIC-15 with confidence intervals and translate the cushioning effect to clinical injury thresholds; (b) multi-direction airbag chambers with selective inflation for lateral and backward falls; (c) field study with elderly volunteers under an extended IRB protocol; (d) multimodal sensing fusion (barometric altitude, surface EMG) for sub-200-ms prediction; (e) on-device personalization via a short calibration walk to reduce the inter-recording variability evident in the LORO confidence interval; (f) deployment of a confirm-to-deploy delay and audible warning to reduce the user-experience cost of false positives.

Acknowledgment

The authors would like to thank the Department of Electrical Engineering and the School of Electrical Engineering, Telkom University, for their support. The authors would also like to thank Sigit Indriyanto and Muhammad Fasha Aqillah for their assistance during data collection and participation in this study.

Funding

This research is funded by Koneksi, Australia's Indonesia Knowledge Partnerships Platform, which is managed by Cowater International Inc. Number: 1447/CRG/2024/42-TelU.

Author Contributions

Cahyadi and Mukhtar conceived and designed the study, coordinated the research activities, collected the data, and contributed to data analysis and interpretation. Cahyadi, Mukhtar, Tang, and Setiyadi contributed to the study design, methodological supervision, and interpretation of the findings. Cahyadi, Mukhtar, and Tang contributed to data analysis, literature review, and manuscript preparation. Cahyadi, Mukhtar, Setiyadi, Puspitasari, and Ramdhani contributed to data interpretation and critically revised the manuscript for important intellectual content. All authors reviewed and approved the final manuscript and agreed to be accountable for all aspects of the work.

Ethical Approval

The protocol was approved under ethics clearance 032/KE.03/SK/03/2025 (Health Research Ethics Committee — National Research and Innovation Agency of Indonesia, March 4th, 2025); subjects gave written informed consent for both data collection and image publication.

Consent To Participate

Written informed consent was obtained from all participants before their inclusion in the study. Participation was voluntary, and participants were informed of their right to withdraw from the study at any time without consequences.

Manuscript received 8 April 2025; Revised 10 June 2025;; Accepted 15 June 2025; Available online 27 June 2025
DOI: https://doi.org/10.35882/ijeeemi.v6i3.407

Consent for Publication

All participants provided written informed consent for the publication of anonymized and aggregated research data. The manuscript contains no personally identifiable information.

Competing Interests

The authors declare no financial or non-financial competing interests that could have influenced the conduct, analysis, interpretation, or reporting of this study.

References

[1] Badan Pusat Statistik (Central Bureau of Statistics), "Statistik Penduduk Lanjut Usia 2023," 2023. Accessed: Sep. 26, 2025. [Online]. Available: https://www.bps.go.id/id/publication/2023/12/29/5d308763ac29278dd5860fad/statistik-penduduk-lanjut-usia-2023.html

[2] R. Tanwar, N. Nandal, M. Zamani, and A. A. Manaf, "Pathway of Trends and Technologies in Fall Detection: A Systematic Review," Healthcare, vol. 10, no. 1, p. 172, Jan. 2022, doi: 10.3390/healthcare10010172.

[3] World Health Organization (WHO), WHO global report on falls prevention in older age. Geneva: World Health Organization, 2008. Accessed: Sep. 30, 2025. [Online]. Available: https://www.who.int/publications/i/item/9789241563536

[4] M. Ibrahim, S. Shawish, S. Aldroubi, A. Dawoud, and W. Abdin, "Airbag Protection and Alerting System for Elderly People," Applied Sciences (Switzerland), vol. 13, no. 16, Aug. 2023, doi: 10.3390/app13169354.

[5] A. J. N. Deniro, N. N. Sulistiawati, and N. Widajanti, "Hubungan antara Usia dan Aktivitas Sehari-Hari dengan Risiko Jatuh Pasien Instalasi Rawat Jalan Geriatri," Jurnal Penyakit Dalam Indonesia, vol. 4, no. 4, p. 199, Dec. 2017, doi: 10.7454/jpdi.v4i4.156.

[6] E. B. Hitcho et al., "Characteristics and circumstances of falls in a hospital setting," J. Gen. Intern. Med., vol. 19, no. 7, pp. 732–739, Jul. 2004, doi: 10.1111/j.1525-1497.2004.30387.x.

[7] R. Faraj, B. Popławski, D. Gabryel, T. Kowalski, and K. Hinc, "Adaptive airbag system for increased evacuation safety," Eng. Struct., vol. 270, Nov. 2022, doi: 10.1016/j.engstruct.2022.114853.

[8] J.-W. Noh, K.-B. Kim, J. H. Lee, B.-H. Lee, Y. D. Kwon, and S. Heui Lee, "The elderly and falls: Factors associated with quality of life A cross-sectional study using large-scale national data in Korea," Arch. Gerontol. Geriatr., vol. 73, pp. 279–283, Nov. 2017, doi: 10.1016/j.archger.2017.08.008.

[9] M. Stenhagen, H. Ekström, E. Nordell, and S. Elmståhl, "Accidental falls, health-related quality of life and life satisfaction: A prospective study of the general elderly population," Arch. Gerontol. Geriatr., vol. 58, no. 1, pp. 95–100, Jan. 2014, doi: 10.1016/j.archger.2013.07.006.

[10] Soediponegoro et al., "Pengembangan Sistem Rekognisi Aktivitas Dan Prediksi Jatuh Pada Lansia Menggunakan Sensor IMU (Development of An Activity Recognition And Fall Prediction System In The Elderly Using IMU Sensor)," Jurnal Elektro dan Telekomunikasi Terapan, vol. 11, no. 1, pp. 54–68, Jun. 2024, doi: 10.25124/jett.v11i1.7299.

[11] C. Tang, N. Zakaria, and W. S. Ruznan, "The development of anti-fall functional clothing for elderly," Global Health Journal, vol. 7, no. 4, pp. 175–181, Dec. 2023, doi: 10.1016/j.glohj.2023.10.001.

[12] S. Wang, J. Sun, and S. Liu, "Fall prevention system based on airbag protection and mechanical exoskeleton support," MATEC Web of Conferences, vol. 336, p. 02015, 2021, doi: 10.1051/matecconf/202133602015.

[13] A. Singh, S. U. Rehman, S. Yongchareon, and P. H. J. Chong, "Sensor Technologies for Fall Detection Systems: A Review," Jul. 01, 2020, Institute of Electrical and Electronics Engineers Inc. doi: 10.1109/JSEN.2020.2976554.

[14] H. W. Lach et al., "Falls in the Elderly: Reliability of a Classification System," J. Am. Geriatr. Soc., vol. 39, no. 2, pp. 197–202, Feb. 1991, doi: 10.1111/j.1532-5415.1991.tb01626.x.

[15] C. A. U. Hassan et al., "A Cost-Effective Fall-Detection Framework for the Elderly Using Sensor-Based Technologies," Sustainability (Switzerland), vol. 15, no. 5, Mar. 2023, doi: 10.3390/su15053982.

[16] F. Wu, H. Zhao, Y. Zhao, and H. Zhong, "Development of a wearable-sensor-based fall detection system," Int. J. Telemed. Appl., vol. 2015, 2015, doi: 10.1155/2015/576364.

[17] F. A. S. Ferreira De Sousa, C. Escriba, E. G. Avina Bravo, V. Brossa, J. Y. Fourniols, and C. Rossi, "Wearable Pre-Impact Fall Detection System Based on 3D Accelerometer and Subject's Height," IEEE Sens. J., vol. 22, no. 2, pp. 1738–1745, Jan. 2022, doi: 10.1109/JSEN.2021.3131037.

[18] S. M. van der Veen and J. S. Thomas, "A Pilot Study Quantifying Center of Mass Trajectory during Dynamic Balance Tasks Using an HTC Vive Tracker Fixed to the Pelvis," Sensors, vol. 21, no. 23, p. 8034, Dec. 2021, doi: 10.3390/s21238034.

[19] T. Tamura, T. Yoshimura, M. Sekine, M. Uchida, and O. Tanaka, "A wearable airbag to prevent fall injuries," IEEE Transactions on Information Technology in Biomedicine, vol. 13, no. 6, pp. 910–914, Nov. 2009, doi: 10.1109/TITB.2009.2033673.

Manuscript received 8 April 2025; Revised 10 June 2025;; Accepted 15 June 2025; Available online 27 June 2025
DOI: https://doi.org/10.35882/ijeeemi.v6i3.407

[20] D. C. Viano, "History of airbag safety benefits and risks," 2024, Taylor and Francis Ltd. doi: 10.1080/15389588.2024.2315889.

[21] A. Ramachandran and A. Karuppiah, "A Survey on Recent Advances in Wearable Fall Detection Systems," 2020, Hindawi Limited. doi: 10.1155/2020/2167160.

[22] G. Shi, C.-S. Chan, Y. Luo, and G. Zhang, "Development of a Human Airbag System for Fall Protection Using MEMS Motion Sensing Technology," in Proceedings of the 2006 IEEE/RSJ International Conference on Intelligent Robots and Systems, Beijing, China: IEEE, Oct. 2006, p. 5774.

[23] G. Shi, C. S. Chan, W. J. Li, K. S. Leung, Y. Zou, and Y. Jin, "Mobile human airbag system for fall protection using mems sensors and embedded SVM classifier," IEEE Sens. J., vol. 9, no. 5, pp. 495–503, May 2009, doi: 10.1109/JSEN.2008.2012212.

[24] Q. Zhang, H. Q. Li, Y. K. Ning, D. Liang, and G. Zhao, "Design and realization of a wearable hip-airbag system for fall protection," in Applied Mechanics and Materials, 2014, pp. 667–674. doi: 10.4028/www.scientific.net/AMM.461.667.

[25] S. Ahn et al., "Optimization of a pre-impact fall detection algorithm and development of hip protection airbag system," Sensors and Materials, vol. 30, no. 8, pp. 1743–1752, 2018, doi: 10.18494/SAM.2018.1876.

[26] E. S. Sanchez, D. C. Zamora, and J. Kim, "Development of Airbag Fabrication Machine and Process for Physical Human Machine Interaction," in 2nd IEEE International Conference on Soft Robotics (RoboSoft), Seoul: IEEE, Apr. 2019, pp. 502–508.

[27] X. Zhang, Z. Xue, and W. Tu, "Design and Performance Research of a Wearable Airbag for the Human Body," Applied Sciences (Switzerland), vol. 13, no. 6, Mar. 2023, doi: 10.3390/app13063628.

[28] O. K. Botonis et al., "Wearable airbag technology and machine learned models to mitigate falls after stroke," J. Neuroeng. Rehabil., vol. 19, no. 1, Dec. 2022, doi: 10.1186/s12984-022-01040-4.

[29] L. Chen, D. Mao, and Q. Gao, "Design and Analysis of the Human Airbag," in Mechanisms and Machine Science, Springer Science and Business Media B.V., 2021, pp. 133–138. doi: 10.1007/978-3-030-64690-5_13.

[30] G. Shi, C.-S. Chang, G. Zhang, W. J. Li, P. H. W. Leong, and K.-S. Leung, "Towards a Mobile Airbag System Using MEMS Sensors and Embedded Intelligence," in 2007 IEEE International Conference on Robotics and Biomimetics, Sanya, China: IEEE, Dec. 2008, p. 2314.

[31] Y. Lee et al., "Experimental Verification of Fall Simulation and Wearable Protect Airbag," in Proceedings of the 4th International Conference on Information and Communication Technologies for Ageing Well and e-Health (ICT4AWE 2018), Madeira: SCITEPRESS, Mar. 2018, pp. 215–218. doi: 10.5220/0006785202150218.

[32] C. Shing Chan et al., "A Human-Airbag System for Hip Protection Using MEMS Motion Sensors: Experimental Feasibility Results," in 2006 IEEE International Conference on Mechatronics and Automation, Luoyang, China: IEEE, Jun. 2006, pp. 831–836.

[33] B. Jo et al., "Design of wearable airbag with injury reducing system," in ICT4AWE 2017 - Proceedings of the 3rd International Conference on Information and Communication Technologies for Ageing Well and e-Health, SciTePress, 2017, pp. 188–191. doi: 10.5220/0006365401880191.

[34] K. Fukaya and M. Uchida, "Protection against Impact with the Ground Using Wearable Airbags," Ind. Health, vol. 46, pp. 59–65, 2008.

[35] S. S. Suprapto, V. A. Kusuma, A. A. Firdaus, W. H. Putra, and R. J. Yuniar, "Design and build an airbag system for elderly fall protection using the mpu6050 sensor module," International Journal of Reconfigurable and Embedded Systems, vol. 13, no. 1, pp. 111–116, Mar. 2024, doi: 10.11591/ijres.v13.i1.pp111-116.

[36] S. N. Robinovitch et al., "Video capture of the circumstances of falls in elderly people residing in long-term care: an observational study," The Lancet, vol. 381, no. 9860, pp. 47–54, Jan. 2013, doi: 10.1016/S0140-6736(12)61263-X.

[37] H. Jung, B. Koo, J. Kim, T. Kim, Y. Nam, and Y. Kim, "Enhanced algorithm for the detection of preimpact fall for wearable airbags," Sensors (Switzerland), vol. 20, no. 5, Mar. 2020, doi: 10.3390/s20051277.

[38] S. Gelmini, S. Strada, M. Tanelli, S. Savaresi, and A. Guzzon, "Automatic detection of human's falls from heights for airbag deployment via inertial measurements," Autom. Constr., vol. 120, Dec. 2020, doi: 10.1016/j.autcon.2020.103358.

[39] D. J. Mühlematter, N. Wiedemann, Y. Xin, and M. Raubal, "Spatially-aware station based car-sharing demand prediction," J. Transp. Geogr., vol. 114, p. 103765, Jan. 2024, doi: 10.1016/j.jtrangeo.2023.103765.

[40] S. Savaş, "Statistical Feature Engineering for Robot Failure Detection: A Comparative Study of Machine Learning and Deep Learning Classifiers," Sensors, vol. 26, no. 5, p. 1649, Mar. 2026, doi: 10.3390/s26051649.

[41] A. M. Yildiz et al., "A novel tree pattern-based violence detection model using audio signals," Expert Syst. Appl., vol. 224, p. 120031, Aug. 2023, doi: 10.1016/j.eswa.2023.120031.

[42] R. Ferrara, M. Giaquinto, G. Percannella, L. Rundo, and A. Saggese, "Personalizing Seizure Detection for Individual Patients by Optimal Selection of EEG

Manuscript received 8 April 2025; Revised 10 June 2025;; Accepted 15 June 2025; Available online 27 June 2025
DOI: https://doi.org/10.35882/ijeeemi.v6i3.407

Signals," Sensors, vol. 25, no. 9, p. 2715, Apr. 2025, doi: 10.3390/s25092715.

[43] P. D. Groves, "Accelerometer measurement model and gravity. ," in Principles of GNSS, Inertial, and Multisensor Integrated Navigation Systems, 2nd ed., Boston: Artech House, 2013, ch. 4.

AUTHOR BIOGRAPHY

Willy Anugrah Cahyadi is a lecturer in the Bachelor of Electrical Engineering Department at Telkom University, who earned his bachelor's and master's degrees in Electrical Engineering and Microelectronics from Institut Teknologi Bandung (ITB), and his doctoral degree (Dr. Eng.) in Information and Communications Engineering from Pukyong National University, Republic of Korea. He is currently a member of the Control, Electronics & Intelligent System (CEIS) research group, focusing on Visible Light Communication (VLC), optical systems, body area networks, and signal processing, with over 60 publications and active involvement in research, curriculum development, and community service in intelligent electro-technological solutions.

Husneni Mukhtar obtained her PhD from the Doctoral School of Electronics, Microelectronics, and Photonics at Université de Strasbourg, France, in 2018. After completing her research at the ICube Laboratory – CNRS–Unistra, France, she began her academic career as a lecturer and researcher at the School of Electrical Engineering, Telkom University, Indonesia. She subsequently led the Renewable Energy and Advanced Electronics Engineering Laboratory (2020–2023) and founded the Advanced Biomedical Intelligent Engineering Laboratory in 2022. She authored several academic textbooks, including Sensor and Actuator with the Cases of Implementation (Tel-U Press, 2022) and Biomedical Physics (Tel-U Press, 2024). Her main research interests include image processing instrumentation for industrial inspection and biomedical analysis, nanometrology, and 3D optical profilometry. She also develops instrumentation and control applications across various engineering domains.

Suto Setiyadi obtained his Bachelor of Engineering (S.T.) degree from Telkom University in 2021 and subsequently received his Master of Engineering (M.T.) degree from the same university in 2023. He began his research at the Microprocessor and Interface Laboratory and the Electronics Laboratory. After completing his undergraduate studies, he worked as a research assistant at Bandung Techno Park. Following his master's graduation, he continued his academic career as a lecturer and researcher at the School of Electrical Engineering, Telkom University, Indonesia. He authored the textbook "Sensor and Actuator with Cases of Implementation" (Tel-U Press, 2022). His primary research interests include biomedical applications of computer vision and embedded systems.

Dita Puspitasari successfully earned a prestigious bachelor's joint degree in Mechatronics Engineering from the International University Liaison Indonesia alongside the Technische Universität Ilmenau in Germany. Advancing her academic expertise, she later completed a master's degree in Materials Science and Engineering from the renowned Bandung Institute of Technology. Currently, Dita serves as a dedicated lecturer in the Biomedical Engineering department at Telkom University, where she actively mentors the next generation of engineers. Her specialized research interests primarily focus on materials science, innovative biomaterials, and advanced biomaterial engineering, aiming to develop impactful solutions at the intersection of technology and healthcare.

Nigel Bryan Tang successfully earned his Bachelor of Engineering degree from Telkom University, Indonesia, in 2025. Demonstrating a strong commitment to advancing his academic and professional career, he is currently pursuing a Master's degree at the prestigious Beijing Institute of Technology, where he is affiliated with the innovative School of Integrated Circuit and Electronics. As a driven researcher, Nigel is highly interested in the cutting-edge development of next-generation wearable devices and advanced sensors. His academic focus heavily encompasses semiconductors and nanotechnology, areas where he aims to contribute meaningful innovations that bridge modern engineering solutions with real-world applications.

Mohamad Ramdhani earned his Bachelor of Engineering in Telecommunication Engineering from STT Bandung in 1999, followed by a Master's Degree in Information Technology from ITT in 2007. Since 2001, he has dedicated his career to academia, serving as a vital lecturer and researcher at Telkom University. Now holding the rank of Associate Professor, he plays a key role in shaping the faculty's academic landscape. His primary research interest lies in the field of Electronics, focusing on innovative technology development. Throughout his extensive tenure, he has remained deeply committed to advancing engineering education and contributing impactful scientific research.

Manuscript received 8 April 2025; Revised 10 June 2025;; Accepted 15 June 2025; Available online 27 June 2025
DOI: https://doi.org/10.35882/ijeeemi.v6i3.407

Indonesian Journal of Electronics, Electromedical Engineering, and Medical Informatics e-ISSN: 2656-8624
Homepage: https://ijeeemi.org/; Vol. 8, No. 3, pp. 391-404, August 2026

Cover Image

Manuscript received 8 April 2025; Revised 10 June 2025;; Accepted 15 June 2025; Available online 27 June 2025
DOI: https://doi.org/10.35882/ijeeemi.v6i3.407